settlements from seismic compression for this case study.

ACKNOWLEDGMENTS

This work was supported primarily by the Pacific Earthquake Engineering Research center (PEER) lifelines program and by the U.S. Geological Survey external research program under contract number G11AP20039. This support is gratefully acknowledged. We also wish to thank Samuel Lasley for providing us a copy of their R code implementing their seismic compression procedure. Any opinions, findings, and conclusions or recommendations expressed in this material are those of the authors and do not necessarily reflect those of the PEER center or the U.S. Geological Survey

REFERENCES

ASTM. (2001). "Standard test methods for maximum index density and unit weight of soils using a vibratory table." D4253, West Conshohoken, Pa.

ASTM. (2006). "Standard test methods for minimum index density and unit weight of soils and calculation of relative density." D5254, West Conshohoken, Pa.

ASTM (2011). "Practices for cycle counting in fatigue analysis." ASTM E1049-85, West Conshohocken, PA.

Duku, P.M., Stewart, J.P., Whang, D.H., and Yee, E. (2008). "Volumetric strains of clean sands subject to cyclic loads." *J. Geotech. Geoenviron. Engrg.*, ASCE, 134 (8), 1073–1085.

Ghayoomi, M., McCartney, J.S., and Ko, H.Y. (2013). "Empirical methodology to estimate seismically induced settlement of partially saturated sand." *J. Geotech. Geoenviron. Engrg.*, ASCE, 139 (3), 367–376.

Hashash, Y.M.A., Musgrove, M.I., Harmon, J.A., Groholski, D.R., Philips, C.A., and Park, D. (2016). "DEEPSOIL 6.1, User Manual".

Idriss, I.M. and Boulanger, R.W. (2008). Soil liquefaction during earthquakes. Monograph MNO-12, Earthquake Engineering Research Institute, Oakland, CA, 261 pp.

Lane, K.S. and Washburn, S.E. (1946). "Capillary tests by capillarimeters and by soil filled tubes." Proc. Highway Research Board, 26, 460–473.

Lasley, S.J., Green, R.A., Chen, Q.S., and Rodriguez-Marek, A. (2016). "Approach for estimating seismic compression using site response analyses." *J. Geotech. Geoenviron. Engrg.*, ASCE, 142 (6), 04016015.

Menq, F.Y. (2003). "Dynamic properties of sandy and gravelly soils." Ph.D. Dissertation, Dept. of Civil Eng., Univ. of Texas, Austin.

Pradel, D. (1998). "Procedure to evaluate earthquake-induced settlements in dry sandy soils." *J. Geotech. Geoenviron. Engrg.*, ASCE, 124 (4), 364–368.

Pyke, R., Seed, H.B., Chan, C.K. (1975). "Settlement of sands under multidirectional shaking." *J. Geotech. Engrg. Div.*, ASCE, 101 (4), 379–398.

Silver, M.L., and Seed, H.B. (1971). "Volume changes in sands during cyclic loading." *J. Soil Mech. Found. Div.*, ASCE, 97 (9), 1171–1182.

Stewart, J.P., Smith, P.M., Whang, D.H., and Bray, J.D. (2002). "Documentation and analysis of field case histories of seismic compression during the 1994 Northridge, California, earthquake." Report No. PEER-2002/09, Pacific Earthquake Engineering Research Center, U.C. Berkeley, Calif.

Stewart, J.P., Smith, P.M., Whang, D.H., and Bray, J.D. (2004). "Seismic compression of two compacted earth fills shaken by the 1994 Northridge earthquake." *J. Geotech. Geoenviron.*

Engrg., ASCE, 130(5), 461–476.
Tokimatsu, K. (2008). “Geotechnical problems in the 2007 Niigata-ken Chuetsu-oki earthquake.” Geotechnical Engineering and Soil Dynamics IV, May 18–22, 2008, Sacramento, CA, ASCE Geotechnical Special Publication No. 181, D. Zeng, M.T. Manzari, and D.R. Hiltunen (eds.), 1–30.
Tokimatsu, K. and Seed, H.B. (1987). “Evaluation of settlements in sand due to earthquake shaking.” *J. Geotech. Engrg*., ASCE, 113(8), 861–878.
Tsukamoto, Y., Ishihara, K. Sawada, S. and Kamo, T. (2004). “Residual deformation characteristics of partially saturated sandy soils subjected to seismic excitation.” Proc. Int. Conf. on Soil Dynamics and Earthquake Engineering, Vol. 1. 694–701.
Wartman, J., Rodriguez-Marek, A., Repetto, P.C., Keefer, D.K, Rondinel, E. Zegarra-Pellane, J., and Baures, D. (2003). “Ground failure.” *Earthquake Spectra*, 19(S1), 35–56.
Wartman, J., Rodriguez-Marek, A., Macari, E. J., Deaton, S., Ramirez-Reynaga, M., Navarro-Ochoa, C, Callan, S., Keefer, D., Repetto, P., and Ovando-Shelley, E. (2005). "Geotechnical aspects of the january 2003 tecoman earthquake." *Earthquake Spectra*, Vol. 21(2), 493–538.
Wu, J. and See, R.B. (2004). “Estimating of liquefaction-induced ground settlement (case studies).” Proc. 5th Int. Conf. on Case Histories in Geotech. Engrg., New York.
Yee, E., Stewart, J.P., and Tokimatsu, K., (2013). “Elastic and large-strain nonlinear seismic site response from analysis of vertical array recordings.” *J. Geotech. Geoenviron. Engrg*., ASCE, 139 (10), 1789–1801.
Yee, E., Duku, P.M, and Stewart, J.P. (2014). “Cyclic volumetric strain behavior of sands with fines of low plasticity.” *J. Geotech. Geoenviron. Engrg*., ASCE, 140 (4), 10pp.
Youd, T.L. (1972). “Compaction of sands by repeated shear straining.” *J. Soil Mech. Found. Div*., ASCE, 98 (7), 709–725.

Advanced Data Analysis of Downhole Seismic Records

Sungmoon Hwang[1]; Farnyuh Menq, Ph.D.[2]; Kenneth H. Stokoe II, P.E., Ph.D.[3]; Richard C. Lee, Ph.D.[4]; and Julia N. Roberts, Ph.D.[5]

[1]Dept. of Civil, Architectural, and Environmental Engineering, Univ. of Texas at Austin, 301 E. Dean Keeton St., Austin, TX 78712. E-mail: syongmoon@utexas.edu
[2]Dept. of Civil, Architectural, and Environmental Engineering, Univ. of Texas at Austin, 301 E. Dean Keeton St., Austin, TX 78712. E-mail: fymenq@utexas.edu
[3]Dept. of Civil, Architectural, and Environmental Engineering, Univ. of Texas at Austin, 301 E. Dean Keeton St., Austin, TX 78712. E-mail: k.stokoe@mail.utexas.edu
[4]Los Alamos National Laboratory, Earth and Environmental Sciences Division, PO Box 1663, Los Alamos, NM 87545. E-mail: rclee@lanl.gov
[5]Dept. of Civil, Architectural, and Environmental Engineering, Univ. of Texas at Austin, 301 E. Dean Keeton St., Austin, TX 78712. E-mail: jnroberts@utexas.edu

ABSTRACT

Downhole seismic testing is commonly used to determine constrained compressional wave and shear wave velocity profiles in geotechnical earthquake engineering investigations. Wave velocities are calculated based on arrival times selected from the original or filtered time records. However, selecting the arrival times can be subjective for reasons such as signal clarity, mechanical and electrical interferences, and significant attenuation with depth. These factors can create inconsistencies in arrival time selections which may result in disputes between the original analyzers and reviewers. In this study, the use of the integrated continuous wavelet transform (ICWT) method is investigated for use in analyzing downhole seismic records. Results using the ICWT method are compared with those obtained from conventional visual "picks". The ICWT method applies continuous wavelet transform to interpret direct arrival measurements. The key feature of the method is transferring a nonlinear sinusoidal-like signal to a linear phase angle plot. Peaks in the recorded signal are shown as 0°, and troughs are shown as phase angle of 180°. By selecting the time point of 0- or 180-degrees with an amplitude above a selected threshold value, the arrival time of first peaks or troughs can be uniquely identified.

INTRODUCTION

In downhole seismic testing, vertical changes of the compression (P) and shear (S) seismic wave velocities are evaluated by locating P- and S- wave seismic sources near the top of a borehole and measuring travel times at numerous intervals with a 3-component sensor in the borehole (ASTM D7400-08). Both P-wave and S-wave velocity profiles can be determined by downhole seismic testing. In geotechnical engineering, P-wave and S-wave velocity profiles are required in earthquake analyses of geotechnical, structural and infrastructure systems as well as in the design of dynamically-loaded machine foundations.

Travel-times are calculated based on arrival times selected from the recorded time signal. Digital filters are often used to facilitate the selection of arrival times by removing unwanted mechanical and electrical interferences. However, selecting the arrival time on a seismic waveform can be difficult. The Continuous Wavelet Transform (CWT) provides an easy way to interpret direct arrival measurements by (1) separating a recorded time signal into at time-frequency plot (spectrogram) and (2) transferring a nonlinear sinusoidal-like signal to a linear phase angle plot. The Integrated Continuous Wavelet Transform (ICWT) method utilizes both the amplitude and phase outputs from the CWT to select the arrival times of the recorded signals by selecting the time point of 0 or 180-degrees with an amplitude above a selected threshold value (Menq et al. 2017).

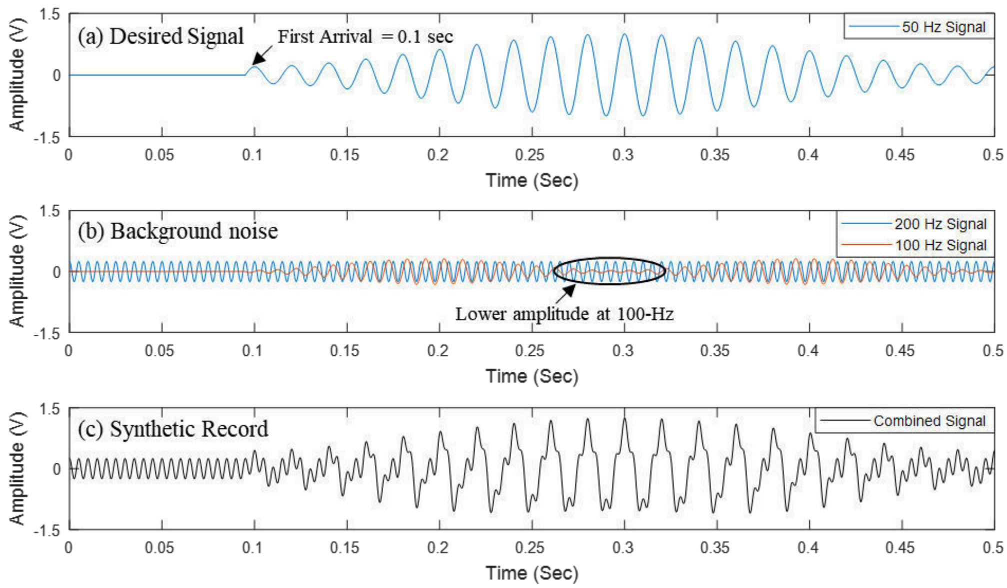

Figure 1. Synthetic time record with primary signal and background noise

In this paper, the benefit of the ICWT method is first illustrated with a synthetic signal. As an example, downhole seismic records obtain from a borehole at a test site in New Mexico are then used for comparisons between the traditional visual selection method and the ICWT method.

INTEGRATED CONTINUOUS WAVELET TRANSFORM (ICWT)

A wavelet is a small, local, wave-like function. In mathematics, a continuous wavelet transform (CWT) is used to divide a time signal into wavelets of various scales along the time axis. The outputs of the CWT are called wavelet coefficients. Generally, scales are expressed in Fourier frequency and the wavelet coefficients are shown in 3-D time-frequency plots (Addison, 2002).

To illustrate the ICWT method for identifying the arrival time, a synthetic time record was created by adding high frequency noise to a 50-Hz sinusoidal wave. The 50-Hz sinusoidal wave signal is shown in Figure 1(a). The high frequency noise signals of 100 and 200 Hz are shown in Figure 1(b). The combined time record is shown in Figure 1(c). It should be noted that the 200-Hz signal has a constant amplitude throughout while the amplitudes of both the 50- and the 100-Hz signals vary with time. As shown in Figure 1(a), the arrival time of the first pulse (peak) is set numerically at 0.1 seconds. Once the high frequency noise at 100- and 200-Hz are added to the signal in Figure 1(c), however, the location of the first peak in the 50-Hz sinusoidal wave is difficult to identify visually.

The CWT outputs of the synthetic time record using a complex Paul Wavelet are shown in Figure 2. The synthetic time record is shown again in Figure 2(a) for reference. The CWT outputs of a complex wavelet contain both real and imagery parts, which can be expressed in terms of amplitude and phase as shown in Figures 2(b) and 2(c), respectively (Torrence and

Compo, 1998). The output from the CWT in Figure 2(b) shows the variation in the amplitude of the synthetic time record as a function of frequency along the y-axis and of time along the x-axis. Variation in amplitude is represented on this graph using a color scale ranging from dark blue (0.0 V) to yellow (1.0 V). Using this method, energy at frequencies of 50-, 100-, and 200-Hz are visually separated.

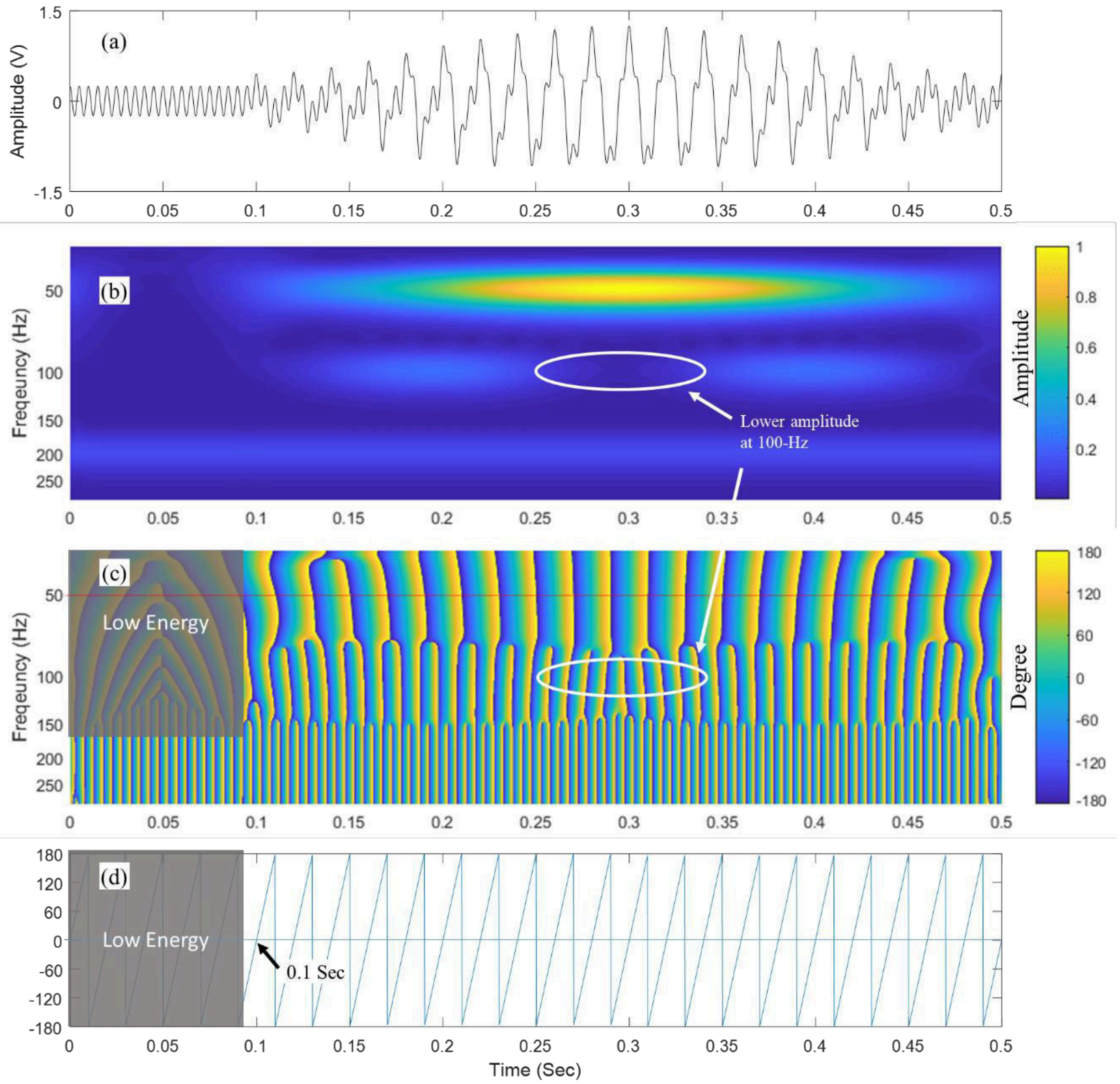

Figure 2. Continuous Wavelet Transform of the synthetic time record

The constant amplitude of 200-Hz signal component can be identified by a horizontal light blue line. The amplitude of the 100-Hz signal can be seen increasing at 0.1 sec, peaking at 0.2 sec, and then decreasing to zero at about 0.3 sec before increasing and peaking again at 0.4 sec and decreasing to zero at 0.5 sec. It creates two distinct horizontal light blue lines corresponding to the portions of the time record. These temporal variations in the 100-Hz signal that are seen in the CWT output cannot be seen in the time record shown in Figure 2(a). The 50-Hz signal can be seen increasing at 0.1 sec, peaking at 0.3 sec, and the decreasing to zero at about 0.5 sec. The CWT method provides an easy way to separate frequency contents of a time signal along the time axis.

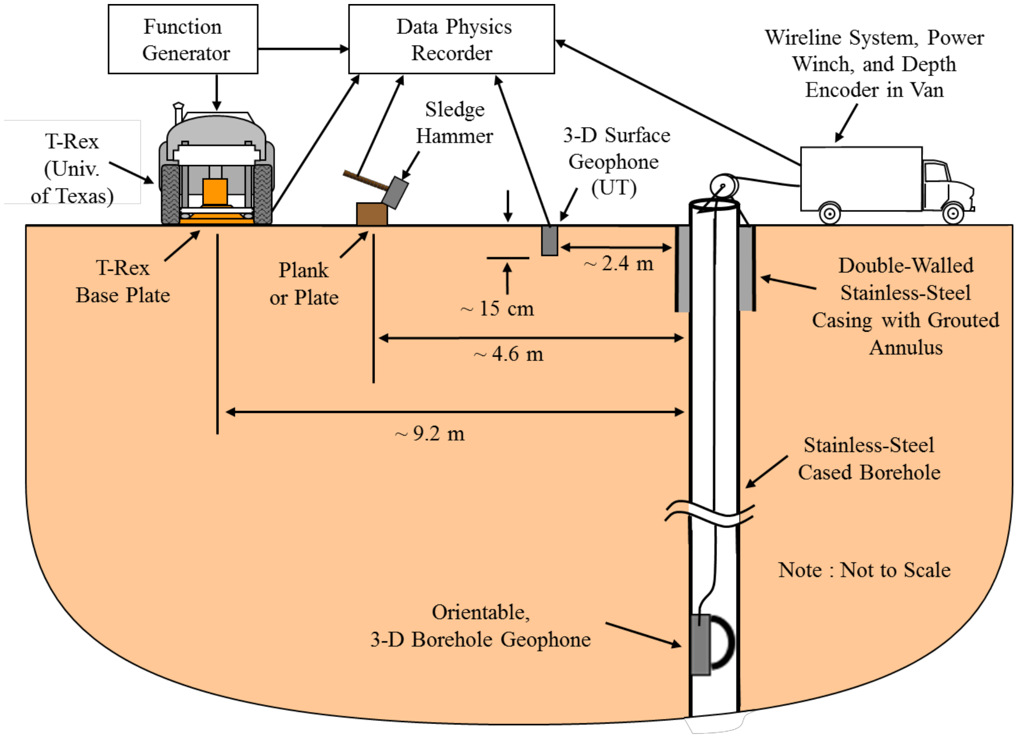

Figure 3. Generalized field setup for downhole seismic measurements at the LANL site

The CWT phase time frequency plot is shown in Figure 2(c). As presented in the figure, a –180 degrees is plotted in blue and a +180 degrees is plotted in yellow. By comparing Figure 2(a) and 2(c), the peaks in the time record are shown with phase angles of 0 degrees on the CWT phase plot, and troughs are shown with phase angles jump between −180 and +180 degrees. The cycles of the 50-, 100-, and 200-Hz signals can be clearly observed in Figure 2(c). In each cycle, phase angle varies from −180 to +180 degrees. As there is no 50- and 100-Hz energy below 0.1 sec, the phase angle in this region appears to be irregular. Similarly, the phase angle around the 100-Hz range also shows an irregular pattern between 0.25 and 0.35 sec where the amplitude of the 100-Hz signal decreases close to nearly zero.

The ICWT method utilizes both the amplitude and phase components of the CWT outputs to select the arrival time. The cross section of the CWT phase time plot at 50 Hz is shown in Figure 2(d). The low energy part of the figure is shown in gray based on the amplitude output. The arrival time of the first peak corresponds to the first 0 degree phase angle after the gray area, which is at 0.1 sec. This analyses method has the unique benefit of using a complex wavelet that, instead of selecting arrival time from a sinusoidal curve shown in Figure 2(a), one can determine an arrival time from the phase angle plot shown in Figure 2(d). Generally speaking, it is a much simpler task to select a time point of a particular amplitude from a straight line (a linear function) than from a nonlinear sinusoidal curve.

DOWNHOLE SEISMIC TESTING

The generalized setup used in downhole seismic testing is shown in Figure 3. The P and S waves generated during downhole testing were monitored at depth with a 3-D borehole sensor, which often consisted of three geophones. In this example, seismic waves are generated on the ground surface with two types of energy sources. These two types of sources were (1) a hand-operated impulsive source for shallow depths and (2) a hydraulically-operated mobile shaker for deeper depths. The hand-operated impulsive sources generate transient impulses to create P and S waves at the ground surface. Vertical, sledge-hammer blows to a circular, hard-plastic plate were used to generate P waves. Shear waves were generated with horizontal, sledge-hammer blows to a horizontal wooden plank with steel end caps upon which a vertical static load was applied by a heavy truck.

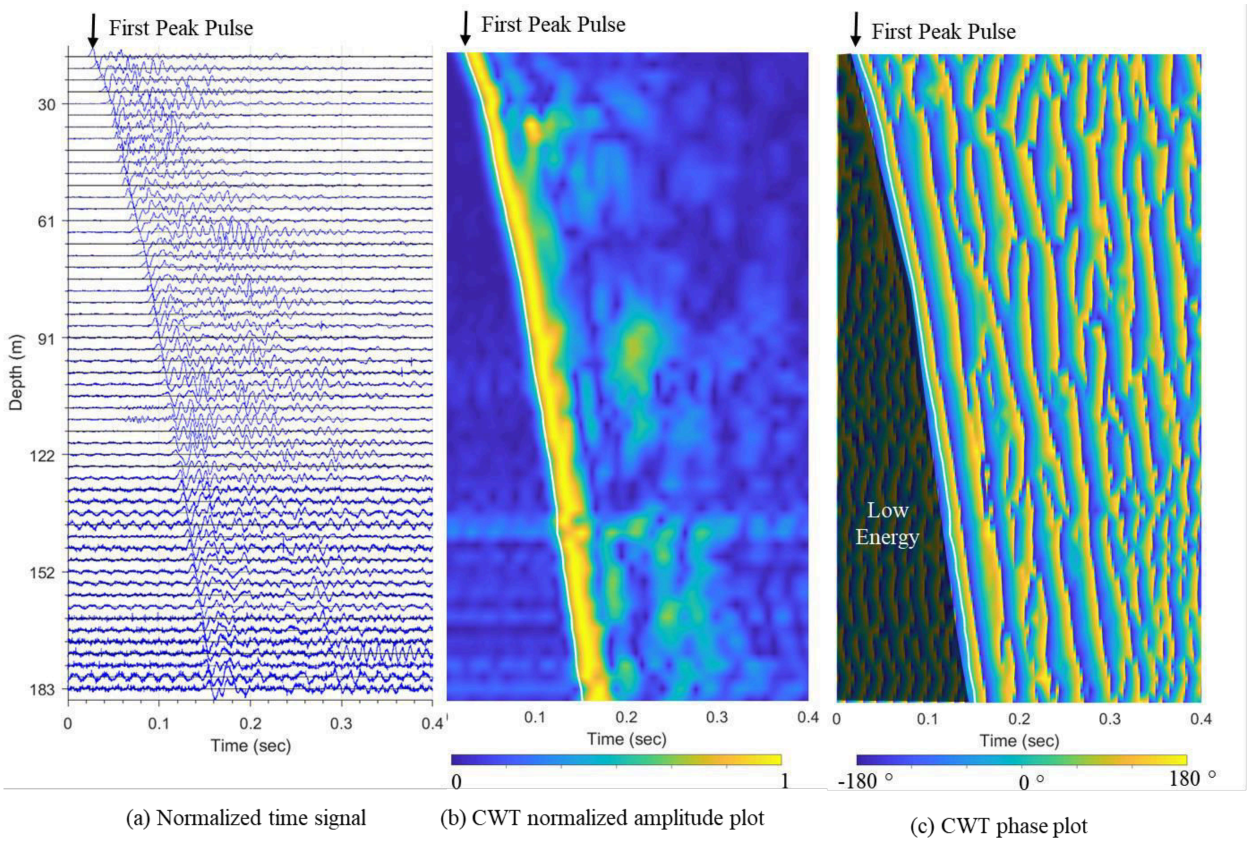

Figure 4. Conventional waterfall, CWT amplitude and phase time vs depth plots between 18 and 183 m

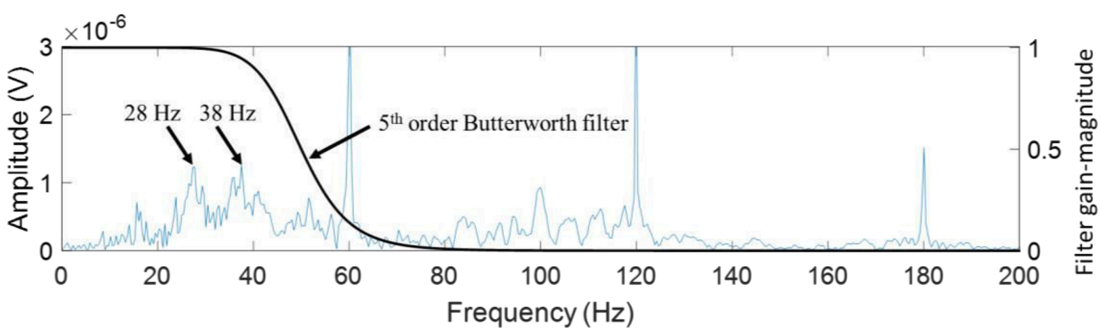

Figure 5. Linear spectra of the time signal recorded at 183 m and the gain-magnitude frequency response of the low-pass filter

The hydraulically-operated mobile shaker used in this study is named T-Rex. It is part of the Natural Hazards Engineering Research Infrastructure Equipment Facility at the University of

Texas at Austin. T-Rex is capable of shaking in 3 directions that include the vertical, horizontal in-line, and horizontal cross-line directions (Stokoe et al., 2016). It is ideal for generating both P-waves (vertical shaking) and S waves (horizontal shaking) for downhole testing. Instead of a pulse signal, ten cycles of a 50-Hz sinusoidal signal were used in the hydraulic mobile shaker tests.

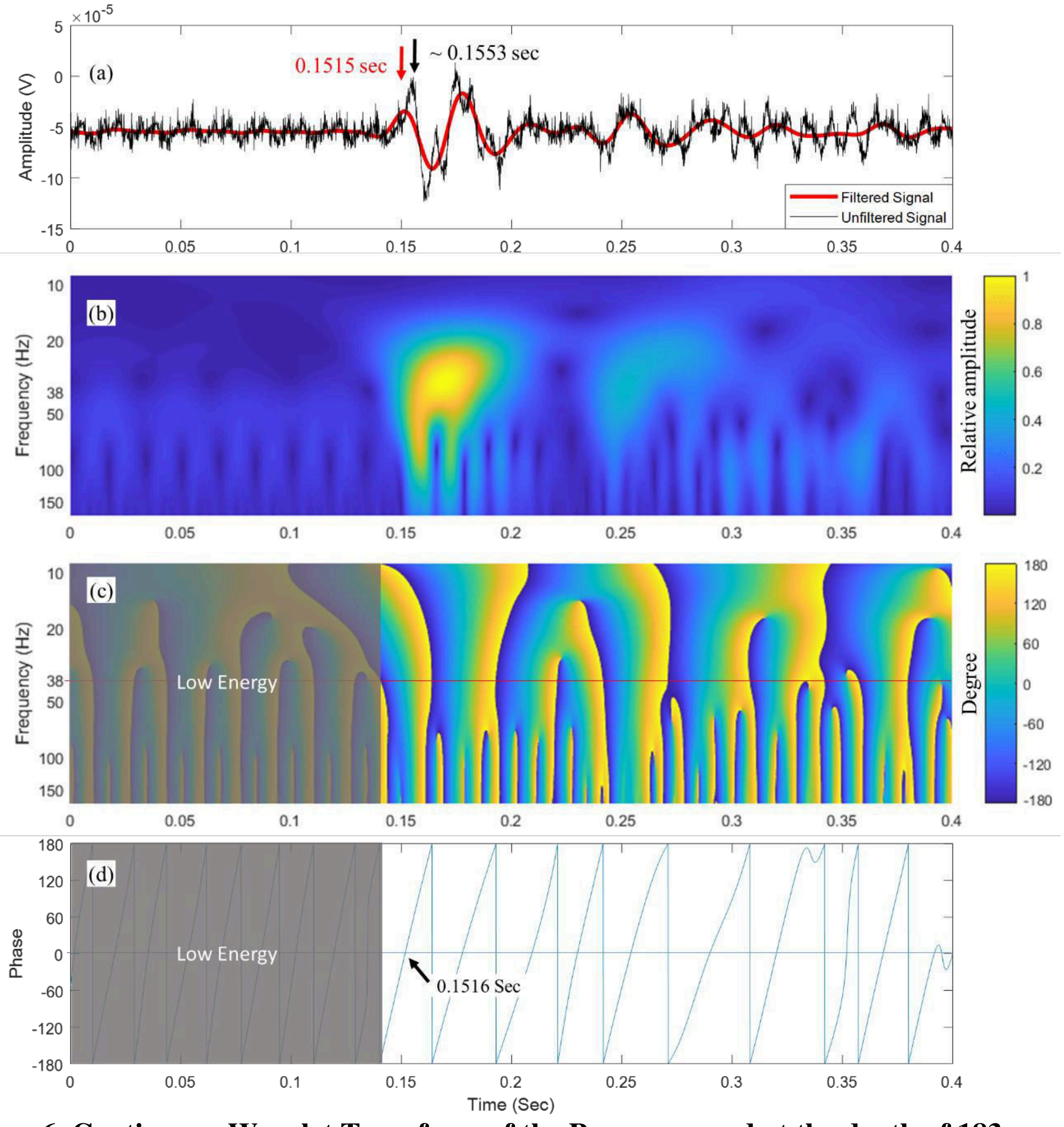

Figure 6. Continuous Wavelet Transform of the P-wave record at the depth of 183 m

Due to space limitations, only results from P-wave measurements are discussed in this article. As the source signals are different in tests using a hand-operated impulsive source and a hydraulic mobile shaker, results from each source type are discussed below in separate sections.

DOWNHOLE TEST WITH A HAND-OPERATED IMPULSIVE SOURCE

The manually-operated seismic sources were used over the depth range of 18 to 183 m, with a 3-m depth increment between measurements. The recorded time signals are presented in Figure 4(a). All signals shown in the plot were normalized by dividing each signal by its maximum amplitude. The arrival time of the first peak can generally be traced down from 18 to 183 m. However, the first arrival peaks can become more difficult to observe at depths of 100 and 113 m. Mechanical interferences obscured the arrival signals at these depths. In addition to the mechanical interferences, electrical interferences (60-Hz power line energy) can be seen at depths below 122 m, which also make it difficult to determine the arrival times at 174, 177, and 180 m.

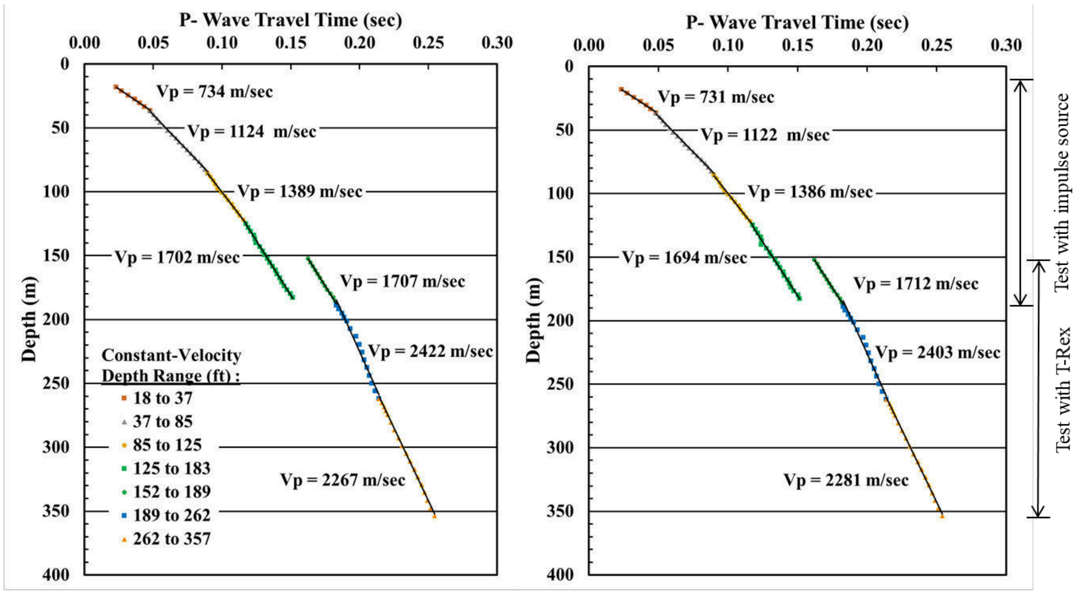

(a) Visual selections (b) Selections from ICWT method

Figure 7. P-wave travel time vs depth plot and resulting P-wave velocity determined by conventional visual "picks" and ICWT method

Traditionally, digital filters are used to remove unwanted interferences. Figure 5 shows the Fast Fourier Transfer (FFT) of the recorded time signal at 183 m. As shown in the figure, the electrical interferences are from the 60-Hz power line and its harmonics at 120- and 180-Hz. To remove these interferences, a zero-phase, 50-Hz low-pass filter (5^{th} order Butterworth) was applied to recorded time signal using the filtfilt function available in MatLab. The gain-magnitude frequency response of the low-pass filter is presented in Figure 5. Figure 6a shows the original and the filtered signals at depth of 183 m. As shown in the figure, the first arrival peak is much easier to identify from the filtered signal. However, the digital filter also shifted the first arrival peak to the left as it removed higher frequency components of the signals. In practice, the same digital filter will be applied to all time records to avoid unwanted effects from the digital filter.

The CWT outputs of the recorded time signal at the depth of 183 m in amplitude and phase time-frequency plots are shown in Figures 6(b) and 6(c), respectively. Similar to the synthetic signal, the first arrival peak is the first, 0-degree line after the low energy zone. It should be noted that the 0-degree line is almost vertical between 38 and 150 Hz as shown in Figure 6(c). For simplicity, the cross-section of the phase time-frequency plot at 38 Hz (approximately the maximum energy zone) is shown in Figure 6(d) for selecting the first arrival peak using the ICWT method. As shown in the figure, the first peak after the low energy zone is located at

0.1516 second.

Figure 6 shows three unique benefits of the ICWT method. First, the ICWT method separates the energy into different frequency regions along the time axis. Users can easily identify the frequency content of the signal of interest. Second, the ICWT method allows arrival times to be determined based on a preselected frequency, which is similar in concept to applying a narrow band pass filter. Third, the ICWT method transfers a nonlinear sinusoidal-like curve to a linear phase angle plot, so the arrival time can be easily and uniquely selected without judgments of the operator.

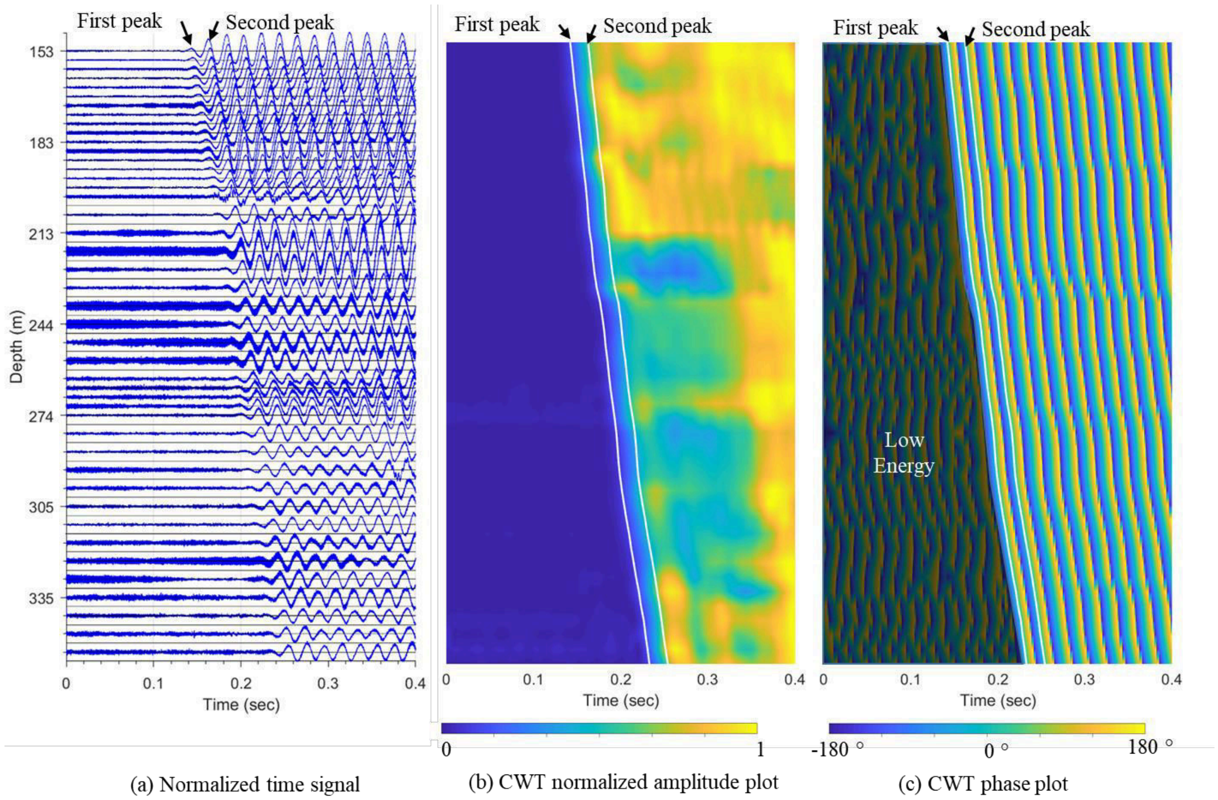

Figure 8. Conventional waterfall plot, CWT normalized amplitude and phase vs depth plot at 50 Hz in the depth range of 153 to 354 m

By combining the cross sections phase plot shown in Figure 6(d) at all test depths, we can generate a 3D-heat-maps-style waterfall plot of the CWT phase outputs as shown in Figure 4(c). Similarly, we can generate a waterfall plot of the CWT amplitude outputs as shown in Figure 4(b). As shown in the figures, the first arrival time along the tested depths can be identified by selecting the green band (0 degree phase) after the low energy zone. The resulting arrival times determined by the visual "picks" and by the ICWT method are shown in Figure 7. P-wave velocities were determined by separating the profile into four layers as presented in the figure. P-wave velocities obtained from the conventional visual "picks" and the ICWT method are nearly the same, with less than 2 % difference. However, the ICWT method took much less time to process the data.

DOWNHOLE TESTING WITH T-REX

With T-Rex, P-waves were generated by shaking in the vertical direction with ten cycles of